HRX-SAFT Equation of State for Fluid Mixtures: Application to Binary Mixtures of Carbon Dioxide, Water, and Methanol

S. B. Kiselev* and J. F. Ely

Chemical Engineering Department, Colorado School of Mines, Golden, Colorado 80401-1887

S. P. Tan, H. Adidharma, and M. Radosz

Department of Chemical and Petroleum Engineering, University of Wyoming, Laramie, Wyoming 82071-3295

In this work, we extend the pure fluid crossover statistical associating fluid theory (HRX-SAFT) equation of state (EOS) (Kiselev et al., *Fluid Phase Equilib.* **2001**, *183*−*184*, 53) to fluid mixtures of polar and associating components. HRX-SAFT incorporates non-analytic scaling laws in the critical region and is transformed into the analytical, classical HR-SAFT EOS far away from the critical point. Pure CO_2, H_2O, and CH_3OH are modeled as associating chain molecules with two association sites (i.e., model 2B). For all three pure substances, the HRX-SAFT EOS reproduces the vapor pressure data from the triple point to the critical temperature with an average absolute deviation (AAD) of about 1%, the saturated liquid and vapor densities with an AAD of about 1−3%, and the single-phase pressures in the one-phase region with an AAD of about 2−3%. Using classical composition-dependent mixing rules, we have also applied the HRX-SAFT EOS to binary mixtures. For the non-association terms in the classical HR-SAFT, we used the vdW1 mixing rules with one constant binary interaction parameter (k_{ij}). For the mixture association term, we assumed that there is cross association between the carbon dioxide oxygens and the hydrogens in methanol and water. The HRX-SAFT mixture model was tested against extensive experimental data for VLE, *PVTx*, and excess properties in carbon dioxide + water, carbon dioxide + methanol, and water + methanol mixtures.

1. Introduction

Strong attractive interactions between molecules in associating fluids impact their thermodynamic and structural properties. Because of this, determining the thermodynamic properties and the phase behavior of mixtures containing associating and hydrogen bonding fluids is an extremely challenging task. The statistical associating fluid theory (SAFT) equations of state (EOS) proposed in the late 1980s by Chapman and co-workers[1−3] and also by Huang and Radosz (HR-SAFT)[4−6] are probably the first molecular-based equations that addressed this problem. Based on the thermodynamic perturbation theory of Werthiem,[9−12] the SAFT equations[1−8] and their different modifications (for a review, see refs 13 and 14) appear to be an effective tool for describing thermodynamic properties and phase equilibria of associating and complex fluids. However, similar to all analytical EOS, the SAFT models are *mean field* equations that fail to reproduce the non-analytical, singular behavior caused by long-scale density fluctuations in the critical region. Therefore, they are incapable of simultaneously reproducing the critical parameters and the vapor−liquid equilibria (VLE), *PVT*, and excess property data in liquid and vapor phases in and beyond the critical region with a single set of molecular parameters. For this purpose, the so-called crossover equations of state[15] should be used.

A general method for incorporating long-range density fluctuations into any classical−analytical equation was proposed by Kiselev.[16] For the last 5 years, this procedure has been successfully applied to different types of equations of state, including cubic,[17−20] SAFT,[21−26] and empirical multi-parameter equations.[27] In this paper, we continue a study initiated in our previous work on the HR-SAFT EOS[22] and develop a crossover, HRX-SAFT, EOS for binary mixtures. First, we have developed a HRX-SAFT EOS for pure carbon dioxide, water, and methanol. Second, using the classical mixing rules in terms of composition, we developed the HRX-SAFT EOS for binary mixtures of carbon dioxide, water, and methanol.

We proceed as follows. In Section 2, we describe the original SAFT EOS for mixtures and describe a general procedure for transforming it into the crossover form. In Section 3, we develop a HRX-SAFT EOS for pure components and binary mixtures and provide an extensive comparison with experimental data. Our results are summarized and discussed in Section 4.

2. Thermodynamic Model

2.1. Classical SAFT Equation of State for Mixtures. A brief description of HR-SAFT for mixtures is given here. The readers are referred to the original paper for details.[6] In SAFT, residual Helmholtz energy is a sum of terms that represent the repulsive and attractive interactions in the system:

$$a^{\mathrm{res}} = \frac{A^{\mathrm{res}}}{n_{\mathrm{m}}RT} = a^{\mathrm{hs}} + a^{\mathrm{disp}} + a^{\mathrm{chain}} + a^{\mathrm{assoc}} \qquad (1)$$

where A is the Helmholtz energy, a is the dimensionless Helmholtz energy, n_{m} is the number of moles, R is the gas constant, T is the absolute temperature, and the superscripts stand for residual, hard-sphere, dispersion, chain, and association, respectively.

For the hard-sphere mixtures, the equation proposed by Mansoori et al.[28] is used:

* To whom correspondence should be addressed: Phone: (303)-273-3190. Fax: (303)273-3730. E-mail: skiselev@mines.edu.

10.1021/ie0512082 CCC: $33.50
Published on Web 04/25/2006

$$a^{\mathrm{hs}} = \frac{6}{\pi\rho N_{\mathrm{A}}}\left[\frac{(\zeta_2)^3 + 3\zeta_1\zeta_2\zeta_3 - 3\zeta_1\zeta_2(\zeta_3)^2}{\zeta_3(1-\zeta_3)^2} - \left(\zeta_0 - \frac{(\zeta_2)^3}{(\zeta_3)^2}\right)\ln(1-\zeta_3)\right] \quad (2)$$

where

$$\zeta_k = \frac{\pi}{6}N_{\mathrm{Av}}\rho\sum_i x_i m_i d_i^k \quad (3)$$

In eqs 2 and 3, N_{Av} is the Avogadro number, ρ is the molar density, m_i is the number of segments of component i, d_i is the temperature-dependent segment diameter of component i, and x_i is the mole fraction of component i.

In HR-SAFT, the dispersion term proposed by Chen and Kreglewski[29] is used:

$$a^{\mathrm{disp}} = \left(\sum_i x_i m_i\right)\sum_{m=1}^{4}\sum_{n=1}^{9} D_{mn}\left(\frac{u}{kT}\right)^m\left(\frac{\zeta_3}{\tau}\right)^n \quad (4)$$

where $\tau = 0.74048$, D_{mn} values are universal constants,[4] and

$$\frac{u}{kT} = \frac{\sum_i\sum_j x_i x_j m_i m_j\left[\frac{u_{ij}}{kT}\right](v^{\mathrm{o}})_{ij}}{\sum_i\sum_j x_i x_j m_i m_j (v^{\mathrm{o}})_{ij}} \quad (5)$$

$$(v^{\mathrm{o}})_{ij} = \left[\frac{1}{2}[(v^{\mathrm{o}})_i^{1/3} + (v^{o})_j^{1/3}]\right]^3 \quad (6)$$

$$u_{ij} = (1-k_{ij})(u_i u_j)^{1/2} \quad (7)$$

Here, k_{ij} is the binary interaction parameter fitted to experimental data and $(v^{\mathrm{o}})_i$ is the temperature-dependent segment volume of pure component i in a closed-packed arrangement.

For the chain term, it is given by

$$a^{\mathrm{chain}} = \sum_i x_i(1-m_i)\ln g^{\mathrm{hs}}(d_i) \quad (8)$$

where $g^{\mathrm{hs}}(d_i)$ is the radial distribution function for hard-sphere fluid mixtures evaluated at contact

$$g^{\mathrm{hs}}(d_i) = \frac{1}{1-\zeta_3} + \frac{3d_i}{2}\frac{\zeta_2}{(1-\zeta_3)^2} + 2\left[\frac{d_i}{2}\right]^2\frac{(\zeta_2)^2}{(1-\zeta_3)^3} \quad (9)$$

To calculate the fractions of nonbonded associating molecules and their derivatives, we use the generalized procedure by Tan et al.[30] The association term is written as

$$a^{\mathrm{assoc}} = \sum_{i=1}^{n} x_i\sum_{j=1}^{s} S_i^j(\ln(X_i^j) - (1/2)X_i^j + (1/2)) \quad (10)$$

where the fraction of associating molecules i not bonded at site j is given by the mass-action equation:

$$X_i^j = \frac{1}{1 + \rho N_{\mathrm{A}}\sum_{k=1}^{n} x_k\sum_{l=1,\,l\neq j}^{s} S_k^l X_k^l \Delta_{ki}^{lj}}, \quad i = 1, ..., n;\ j = 1, ..., s \quad (11)$$

In eqs 10 and 11, S_i^j is the number of association sites of type j in each molecule of component i, n is the number of components in the mixture, and s is the number of association-site types. Δ_{ki}^{lj} is the association strength between site type l in component k and site type j in component i and is approximated by[1]

$$\Delta_{ki}^{lj} = \kappa_{ki}^{lj} g^{\mathrm{hs}}(\sigma_{ki})\left(\exp\left(\frac{\epsilon_{ki}^{lj}}{kT}\right) - 1\right) \quad (12)$$

where κ_{ki}^{lj} is a measure of the volume available for bonding between site of type l in component k with site of type j in component i, ϵ_{ki}^{lj} is the well depth of the site−site interaction potential between site of type l in component k with site of type j in component i, $g^{\mathrm{hs}}(\sigma_{ki})$ is the hard-sphere pair correlation function evaluated at contact, and σ_{ki} is the cross segment diameter.

The advantage of the generalized procedure used in this work is that the high-order derivatives of X_i^j are very simple to obtain and can be written in a matrix form:

$$[\Lambda_{pq}]\left[\frac{\partial^m}{\partial y_1\,\partial y_2 \cdots \partial y_m}[X_i^j]\right] = [\Psi_p^{\,y_1 y_2 \cdots y_m}] \quad (13)$$

where the matrix $[\Lambda_{pq}]$ has an order of $(s \times n) \times (s \times n)$ with

$$p = n(j-1) + i \quad i = 1, ..., n;\ j = 1, ..., s$$
$$q = n(l-1) + k \quad k = 1, ..., n;\ l = 1, ..., s \quad (14)$$

and the other two matrices have the order of $(s \times n) \times 1$. As described in Tan et al.,[30] the elements of matrix $[\Lambda_{pq}]$ do *not* depend on variables y_n, but those of matrix $[\Psi_p^{\,y_n}]$ do. The expressions of $[\Lambda_{pq}]$ as well as those of matrices $[\Psi]$ for first-order derivatives and commonly used second-order derivatives of X_i^j are given in ref 30. Matrices $[\Psi]$ for the third-order derivatives needed in this work are given in the Appendix.

2.2. Crossover HR-SAFT EOS. The general procedure for transforming an analytical EOS into the crossover form has been described in detail elsewhere.[16,19] Following this approach, we first formally split the dimensionless classical Helmholtz free energy $a(T, v)$ for the HR-SAFT EOS in two contributions:

$$a(T, v) = \Delta a(\Delta T, \Delta v) + a_{\mathrm{bg}}(T, v) \quad (15)$$

where the critical, $\Delta a(\Delta T, \Delta v)$, and background, $a_{\mathrm{bg}}(T, v)$, parts are given by

$$\Delta a(\Delta T, \Delta v) = a^{\mathrm{res}}(\Delta T, \Delta v) - a_0^{\mathrm{res}}(\Delta T) + \bar{P}_0(\Delta T)\Delta v - \ln(\Delta v + 1) \quad (16)$$

$$a_{\mathrm{bg}}(T, v) = a_0^{\mathrm{res}}(T) - \bar{P}_0(T)\Delta v + a^{\mathrm{id}}(T) \quad (17)$$

$\Delta T = T/T_{0\mathrm{c}} - 1$ and $\Delta v = v/v_{0\mathrm{c}} - 1$ are dimensionless distances from the classical critical temperature $T_{0\mathrm{c}}$ and molar volume $v_{0\mathrm{c}}$, respectively; $\bar{P}_0(T) = P_0(T, v_{0\mathrm{c}})v_{0\mathrm{c}}/RT$ is the dimensionless pressure; $a_0^{\mathrm{res}}(T) = a^{\mathrm{res}}(T, v_{0\mathrm{c}})$ is the dimensionless residual part of the Helmholtz energy along the critical isochore $v = v_{0\mathrm{c}}$; and $a^{\mathrm{id}}(T)$ is the dimensionless temperature-dependent ideal gas Helmholtz free energy.

In the second step, we replace the classical values of ΔT and Δv in the critical part $\Delta a(\Delta T, \Delta v)$ with the renormalized values:[22,31]

$$\bar{\tau} = \tau Y^{-\alpha/2} + (1+\tau)\Delta T_c Y^{2(2-\alpha)/3} \quad (18)$$

$$\bar{\varphi} = \varphi Y^{(\gamma-2\beta)/4} + (1+\varphi)\Delta v_c Y^{(2-\alpha)/2} \quad (19)$$

where $\alpha = 0.11$, $\beta = 0.325$, and $\gamma = 2 - 2\beta - \alpha = 1.24$ are universal nonclassical critical exponents;[32,33] $\tau = T/T_c - 1$ is a dimensionless deviation of the temperature from the true critical temperature T_c; $\varphi = v/v_c - 1$ is a dimensionless deviation of the molar volume from the true critical molar volume v_c; $\Delta T_c = (T_c - T_{0c})/T_{0c} \ll 1$ and $\Delta v_c = (v_c - v_{0c})/v_{0c} \ll 1$ are dimensionless shifts of the critical temperature and volume, respectively; and $Y(q) = \mathrm{Y}(q)^{1/\Delta_1}$ denotes a crossover function, where $\mathrm{Y}(q)$ is a crossover function introduced in our previous works.[22,31,34]

In this work we use a simple phenomenological expression for the crossover function $Y(\tau, \varphi)$:

$$Y(q) = \left(\frac{q}{1+q}\right)^2 \quad (20)$$

where the renormalized distance to the critical point q is found from a solution of the crossover sine model (SM):[34]

$$\left(q^2 - \frac{\tau}{Gi}\right)\left[1 - \frac{1}{4}\left(1 - \frac{\tau}{q^2 Gi}\right)\right] = b^2\left\{\frac{\varphi[1 + v_1 \exp(-10\varphi)]}{m_0 Gi^{\beta}}\right\}^2 Y^{1-2\beta} \quad (21)$$

The coefficients m_0, v_1, and the Ginzburg number Gi are system-dependent parameters, while the parameter $b^2 = b_{LM}^2 \cong 1.359$ is a universal linear model (LM) parameter.[34] The crossover SM as given by eq 21 is physically equivalent to the crossover sine model developed earlier[22,31,34] but without the rectilinear term and with a different empirical term $\propto v_1 \exp(-10\varphi)$,[19] which provides the physically obvious condition $Y = 1$ at the liquid triple point. Finally, the HRX-SAFT expression for the Helmholtz free energy can be written in the form:

$$a(T, v) = \Delta a(\bar{\tau}, \bar{\varphi}) - \Delta v \bar{P}_0(T) + a_0^{\mathrm{res}}(T) + a^{\mathrm{id}}(T) \quad (22)$$

The principle of the critical point universality[35−37] implies that, in order to obtain a crossover EOS for mixtures, mixing rules in terms of a "field" variable (the chemical potential of a mixture $\mu = \mu_2 - \mu_1 = (\partial A/\partial x)_{T,v}$) rather than the "density" variable (the composition x) should be used. In this case, the parameters T_c, P_c, and v_c in eqs 18−21 are the real critical parameters of a mixture, determined from the critical-point conditions:

$$\left(\frac{\partial \mu}{\partial x}\right)_{T_c,P_c} = 0, \left(\frac{\partial^2 \mu}{\partial x^2}\right)_{T_c,P_c} = 0, \left(\frac{\partial^2 \mu}{\partial x^2}\right)_{T_c,P_c} > 0 \quad (23)$$

This approach has been used for developing the GCS−FV model for binary mixtures based on a simple cubic EOS, for which the critical conditions, eq 23, can be solved analytically.[19] Unfortunately, this is not a case for the SAFT EOS. Even for pure fluids, the critical parameters in the SAFT EOS can only be found numerically, and evaluation of the critical parameters in mixtures requires special, time-consuming algorithms. It was shown by Kiselev and co-workers,[18,19,34,38] however, that if one is not interested in reproducing all scaling laws asymptotically close to the critical point of a binary mixture, the classical mixing in terms of composition can be used. Thus, in this work we have adopted the mixing rules in terms of composition. In this case the parameters T_c, P_c, and v_c in the HRX-SAFT EOS for mixtures are the pseudo-critical parameters, and the classical critical molar density and temperature (i.e., $\rho_{0c}(x)$ and $T_{0c}(x)$) are obtained by solving the criticality conditions:

$$\left(\frac{\partial P}{\partial \rho}\right)_{x,T_{0c}} = \left(\frac{\partial^2 P}{\partial \rho^2}\right)_{x,T_{0c}} = 0 \quad (24)$$

where the crossover EOS can be obtained by differentiation of eq 22 with respect to volume:

$$P(v, T, x) = -RT\left(\frac{\partial a}{\partial v}\right)_{x,T} = \frac{RT}{v_{0c}}\left\{-\frac{v_{0c}}{v_c}\left(\frac{\partial \Delta a}{\partial \varphi}\right)_{x,T} + \bar{P}_0(T)\right\} \quad (25)$$

Once ρ_{0c} and T_{0c} are known, the critical pressure P_{0c} can be also obtained.

Table 1. System-Dependent Parameters in the HRX-SAFT EOS for Pure Components

parameter	CO_2	H_2O	CH_3OH
v^{oo} (mL·mol^{-1})	7.61186616	1.18482926·10^1	1.14021730·10^1
m	2.59046832	1.23627004	2.02399874
u^0/k_B (K)	1.50368095·10^2	3.18950112·10^2	1.90936260·10^2
ϵ/k_B (K)	1.07689612·10^3	2.86888707·10^3	2.74216117·10^3
κ	8.79956038·10^{-3}	4.96889665·10^{-2}	5.67861645·10^{-2}
Gi	6.10904160·10^{-2}	3.41091396·10^{-1}	1.82406957·10^{-1}
M_w	44.010	18.0152	32.0420
T_c (K)[a]	304.120	647.096	512.750
ρ_c (mol·L^{-1})[a]	10.7625	17.8738	8.27000
P_c (bar)[b]	73.3650	220.619	81.1849

[a] Experimental values adopted from Table 1 in ref 19. [b] Calculated with the HRX- SAFT EOS.

3. Comparison with Experimental Data

3.1. Pure Components. To apply the HRX-SAFT EOS to mixture calculations, one needs first to know the pure component parameters. The HRX-SAFT EOS for pure fluids contains five classical parameters (the segment number m, the segment volume v^{oo} (or σ), the segment energy u^o, the well depth of site−site potential ϵ, and the volume bonding parameter κ) and three crossover parameters (the coefficients m_0, v_1, and the Ginzburg number Gi). To reduce the number of the adjustable parameters and make the model more predictive we set $m_0 = 1$ and expressed the coefficient v_1 in eq 21 as a function of the inverse Ginzburg number $g = Gi^{-1}$:

$$v_1 = v_{01} g\left(1 - \frac{v_{11} g}{10 + g}\right) \quad (26)$$

where the coefficients $v_{01} = 8.7433 \cdot 10^{-4}$ and $v_{11} = 0.87136$ were found by fitting the HRX-SAFT EOS with vapor−liquid density data for several fluids. After these simplifications, only six parameters remain in the model: m, v^{oo} (or σ), u^o, ϵ, κ, and the Ginzburg number Gi. These parameters were found from fits of the HRX-SAFT EOS to the VLE and one-phase PVT data of the three substances studied in this work. Since the carbon dioxide has a strong quadruple moment, it can form complexes with water and methanol. Therefore, following Button and Gubbins,[39] we also treated carbon dioxide as an associating fluid. All system-dependent parameters for pure carbon dioxide, water, and methanol are listed in Table 1.

Since the results for methanol are very similar to those obtained in our previous work,[22] they are not considered here, but comparisons with experimental data for carbon dioxide and

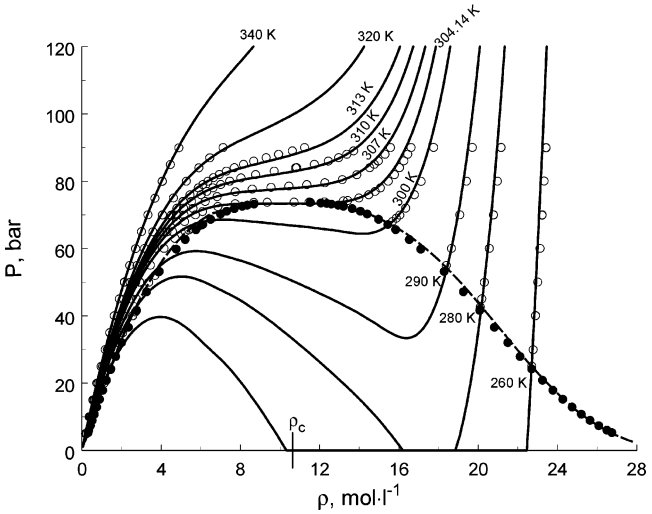

Figure 1. *PρT* data (symbols) for carbon dioxide[53,54] with predictions of the HRX-SAFT model (curves). The empty symbols correspond to the one-phase region, and the filled symbols indicate the VLE data.

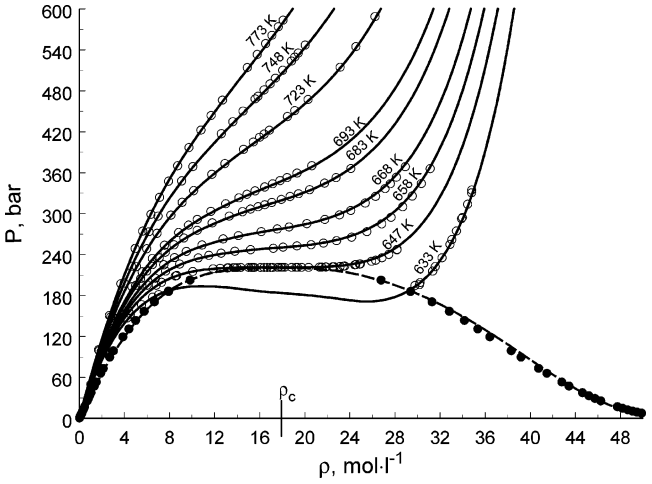

Figure 2. *PρT* data (symbols) for water[55−58] with predictions of the HRX-SAFT model (curves). The empty symbols correspond to the one-phase region, and the filled symbols indicate the VLE data generated with IAPWS-95 Formulation.[40]

water are shown in Figures 1−3. For both fluids, excellent agreement between the HRX-SAFT predictions and experimental VLE and *PVT* data in a wide range of the state parameters, including the nearest vicinity of the critical point, is observed. For all three substances, the HRX-SAFT EOS reproduces the vapor pressure data from the triple point to the critical temperature with an average absolute deviation (AAD) of about 1%, the saturated liquid and vapor densities with an AAD of about 1−3%, and the single-phase pressures in the one-phase region with an AAD of about 2−3%. At lower temperatures the HRX-SAFT EOS heats of vaporization for water deviate by about 5−8% from the values calculated with the IAPWS-95 Formulation.[40] We note however that, since these data were not used for the optimization of the HRX-SAFT EOS, the predictions of the model for ΔH_V shown in Figure 3 are still very reasonable.

3.2. Binary Mixtures. As we mentioned above, we treated pure carbon dioxide as an associating fluids with two non-hydrogen bonding sites:

$$CO_2 \rightleftharpoons O + CO \Rightarrow \begin{cases} \text{site 1} \leftrightarrow O \\ \text{site 2} \leftrightarrow C \end{cases} \tag{27}$$

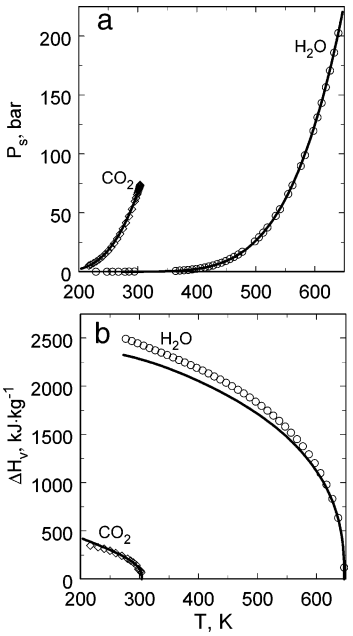

Figure 3. Saturated pressure (a) and latent heat of vaporization (b) data (symbols) for carbon dioxide[59] and water[40] with predictions of the HRX-SAFT model (curves).

and considered the hydrogen bonding type of interaction in methanol

$$CH_3OH \rightleftharpoons H + OH_3C \Rightarrow \begin{cases} \text{site 1} \leftrightarrow O \\ \text{site 3} \leftrightarrow H \end{cases} \tag{28}$$

and water

$$H_2O \rightleftharpoons H + OH \Rightarrow \begin{cases} \text{site 1} \leftrightarrow O \\ \text{site 3} \leftrightarrow H \end{cases} \tag{29}$$

This definition of bonding sites requires us to introduce into the HRX-SAFT EOS model cross-interaction parameters κ_{ki}^{lj} and ϵ_{ki}^{lj}. As one can see from Table 1, the C−O interaction in carbon dioxide is almost three times weaker than the hydrogen bonding interaction in methanol and water. Therefore, for simplicity, for the cross-interaction in the carbon dioxide (1) + methanol (2) and carbon dioxide (1) + water mixtures (2) we set

$$\kappa_{12}^{21} = 0, \quad \epsilon_{12}^{21} = 0 \tag{30}$$

In water and methanol the interaction is hydrogen bonding; therefore, for the cross-interaction parameters in water (1) + methanol (2) mixtures we set

$$\kappa_{12}^{31} = \kappa_{12}^{13}, \quad \epsilon_{12}^{31} = \epsilon_{12}^{13} \tag{31}$$

In both cases, for the Ginzburg number *Gi* and coefficient υ_1 in all mixtures we used simple linear relationships:

$$\frac{1}{Gi(x)} = \frac{1-x}{Gi^{(0)}} + \frac{x}{Gi^{(1)}}, \quad \upsilon_1(x) = \upsilon_1^{(0)}(1-x) + \upsilon_1^{(1)}x \tag{32}$$

(where superscripts "0" and "1" denote the first, $x = 0$, and second, $x = 1$, components of the mixture, respectively), and the coefficients κ_{12}^{13} and ϵ_{12}^{13} were treated as adjustable model parameters. The values of the system-dependent constants in the HRX-SAFT EOS for binary mixtures are listed in Table 2.

Table 2. System-Dependent Parameters in the HRX-SAFT EOS for Mixtures

parameter	CO_2 (1) + CH_3OH (2)	H_2O (1) + CH_3OH (2)	CO_2 (1) + H_2O (2)
k_{12}	$1.0\cdot10^{-1}$	$2.61950491\cdot10^{-2}$	$3.22243815\cdot10^{-1}$
ϵ_{12}^{13}/k_B (K)	$2.74216117\cdot10^{3}$ [a]	$3.03683587\cdot10^{3}$	$8.47738045\cdot10^{2}$
κ_{12}^{13}	$3.0\cdot10^{-3}$	$1.78407468\cdot10^{-2}$	$9.72974521\cdot10^{-1}$

[a] The coefficient $\epsilon_{12}^{13} = \epsilon$ for pure methanol.

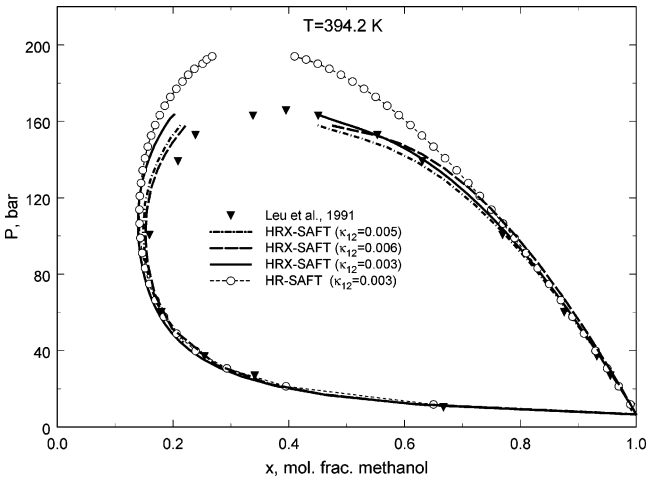

Figure 4. Pressure−composition VLE isotherm for carbon dioxide + methanol mixture. The curves correspond to the HRX-SAFT model with different value of κ_{12}^{13}, the open circles with dashed curves represent the values calculated with the classical HR-SAFT EOS with $\kappa_{12}^{13} = 0.003$, and the filled triangles indicate the experimental data.[41]

3.2.1. Carbon Dioxide + Methanol. The first mixture that we considered was the carbon dioxide + methanol. In this mixture, the coefficient ϵ_{12}^{13} was set equal to the coefficient ϵ_{AB} for pure methanol, and the coefficients k_{12} and κ_{12}^{13} were found from optimization of the HRX-SAFT EOS to the $P-x$ VLE data at $T = 394.2$ K obtained by Leu et al.[41] The comparisons of the experimental data with the values calculated with the HRX-SAFT model with different values of the parameter κ_{12}^{13} are shown in Figure 4. The empty circles with eye-guide lines in Figure 4 represent the values calculated with the classical HR-SAFT EOS with the same set of the parameters as in the HRX-SAFT but with a zero value of the Ginzburg number. As one can see, far away from the critical point at low pressures, both the HRX and HR SAFT equations practically coincide, but the HRX-SAFT EOS gives much better representation of the experimental $P-x$ data in the critical region, where the HR-SAFT gives of about 20−25% higher values of pressure than the experimental ones.

Comparison of the predictions of the HRX-SAFT model with experimental data on other isotherms is shown in Figures 5−7. As one can see, contrary to the HR-SAFT EOS, the HRX-SAFT model not only gives a much better description of the $P-x$ data in the critical region but also reproduces the $P-\rho$ data with a high accuracy. Since no $P-\rho$ data have been used for the optimization of the model, these results indicate the high predictability and thermodynamic self-consistency of the HRX-SAFT EOS for the carbon dioxide + methanol mixture. The little "humps" observed in Figure 6 are the result of the chosen parametrization. As we mentioned above, the more rigorous way of representing the thermodynamic surface of binary mixtures in the critical region is a formulation of the crossover equation of state for mixtures in terms of the field variable μ and not x. Therefore, we were not able to reproduce with the HRX-SAFT EOS experimental data asymptotically close to the critical point. However, it is important to note that, because of the complexity of this mixture, a simultaneous representation of the $P-x$ and $P-\rho$ VLE data have not been achieved even with the field-variable formulated crossover Leung-Griffiths model,[42] and the results presented in Figures 5−7 look rather impressive.

3.2.2. Water + Methanol. For the previous mixture, all mixing parameters were found by fitting isothermal $P-x$ VLE data at 394.2 K and then using those parameters on other isotherms and $P-\rho$ VLE calculations. For the second mixture considered here, the water + methanol mixture, all system-dependent parameters were found from a fit of the HRX-SAFT EOS to the one-phase *PVTx* data obtained by Shahverdiev and Safarov[43] and by Aliev et al.[44] and were then used for calculations of other properties for this mixture. In Figure 8, we show the deviations between experimental and calculated densities for the water + methanol mixture. The empty symbols in Figure 8 indicate the data of Shahverdiev and Safarov,[43] and

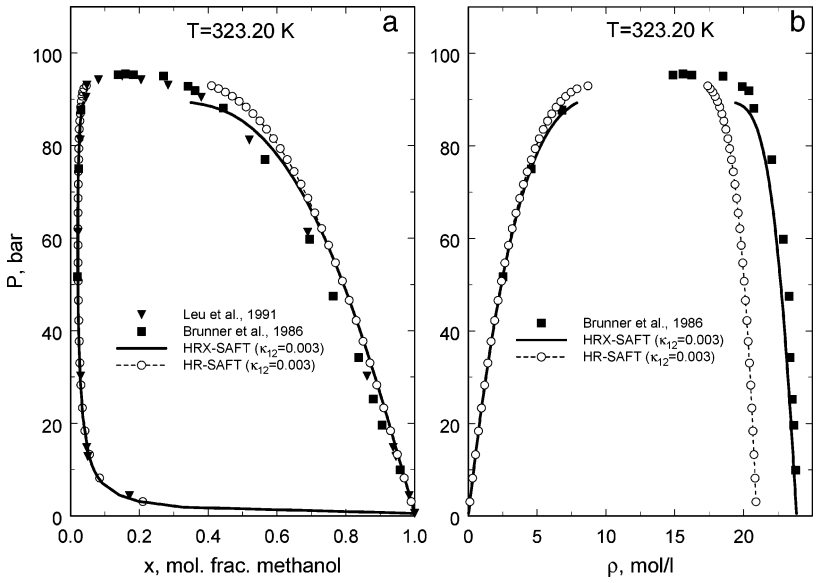

Figure 5. Pressure−composition (a) and pressure−density (b) VLE isotherms for carbon dioxide + methanol mixture. The curves correspond to the HRX-SAFT model with $\kappa_{12}^{13} = 0.003$, the open circles with dashed curves represent the values calculated with the classical HR-SAFT EOS, and the filled triangles indicate the experimental data.[41,60]

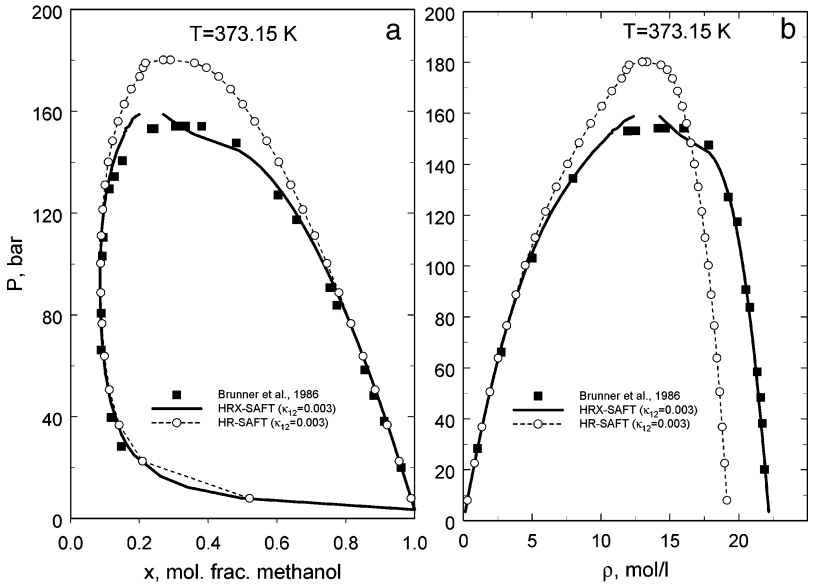

Figure 6. Pressure−composition (a) and pressure−density (b) VLE isotherms for carbon dioxide + methanol mixture. The curves correspond to the HRX-SAFT model with $\kappa_{12}^{13} = 0.003$, the open circles with dashed curves represent the values calculated with the classical HR-SAFT EOS with $\kappa_{12}^{13} = 0.003$, and the filled triangles indicate the experimental data.[60]

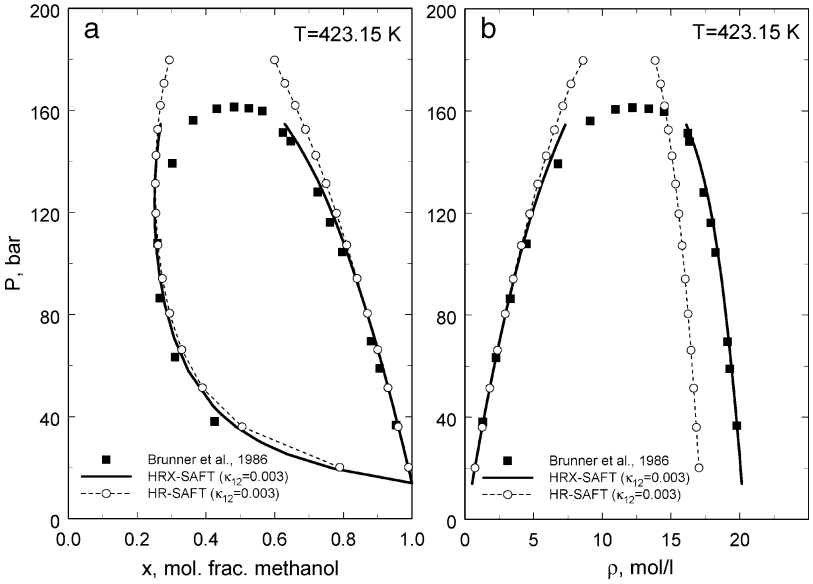

Figure 7. Pressure−composition (a) and pressure−density (b) VLE isotherms for carbon dioxide + methanol mixture. The curves correspond to the HRX-SAFT model with $\kappa_{12}^{13} = 0.003$, the open circles with dashed curves represent the values calculated with the classical HR-SAFT EOS with $\kappa_{12}^{13} = 0.003$, and the filled triangles indicate the experimental data.[60]

the filled symbols correspond to the data obtained by Aliev et al.[44] Up to 2000 bar, the maximum deviations do not exceed 3% and are less than 2% when $P < 1000$ bar. However, because of the steepness of the $P-\rho$ isotherms at low temperatures, these small density deviations can produce large pressure deviations. In Figure 9, we show a comparison of the HRX-SAFT predictions with *PVT* data along several isochors for the 0.64 H_2O + 0.36 CH_3OH mixture reported by Aliev et al.[44] As one can see, at some isochors the systematic deviations between calculated values of pressure and experimental data are observed. The filled symbols in Figure 9 represent the experimental bubble curve data.[44,45] When $T < 420$ K, where the one-phase *PVT* data were used for the optimization, the agreement between the calculated and experimental bubble pressures is very good. However, at high temperatures the HRX-SAFT predictions lie about 15−20% higher than experimental data of Bazaev et al.[46]

In addition to VLE behavior, excess properties of this system are also of practical interest. Comparisons of the HRX-SAFT predictions with experimental excess molar volumes, V_m^E, and the excess molar enthalpy, H_m^E, data for the water + methanol mixtures are shown in Figures 10 and 11. Again, at low temperatures and moderate pressures good agreement of the predicted values and experimental is observed. At higher temperatures the deviations between calculated and experimental values of the excess molar enthalpy are increased.

3.2.3. Carbon Dioxide + Water. The last mixture that was considered in this work is the carbon dioxide + water mixture. In accordance with the classification scheme of van Konynenburg and Scott,[47] the phase behavior of the CO_2 + H_2O mixture belongs to Type III mixtures with a very short liquid−vapor critical locus which starts from the critical point of pure CO_2 and terminates at the upper critical end point. At high temper-

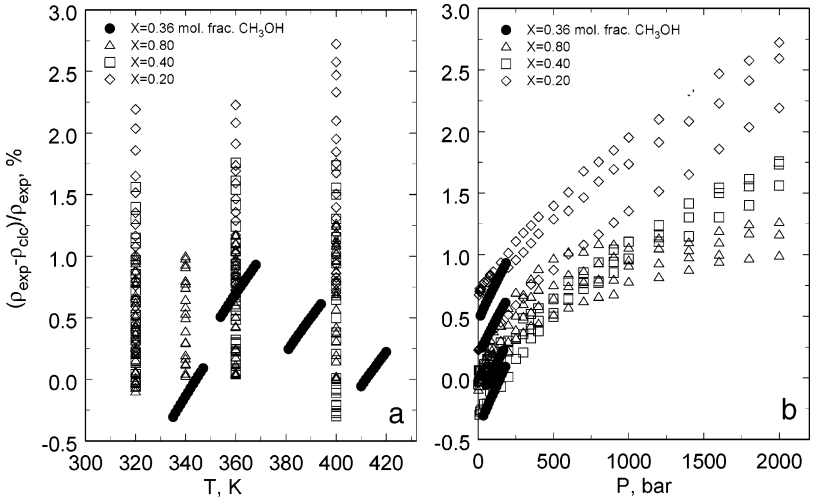

Figure 8. Deviations between experimental densities obtained for water + methanol mixture by Shahverdiev and Safarov[43] (empty symbols) and by Aliev et al.[44] (filled symbols) and the values calculated with the HRX-SAFT EOS.

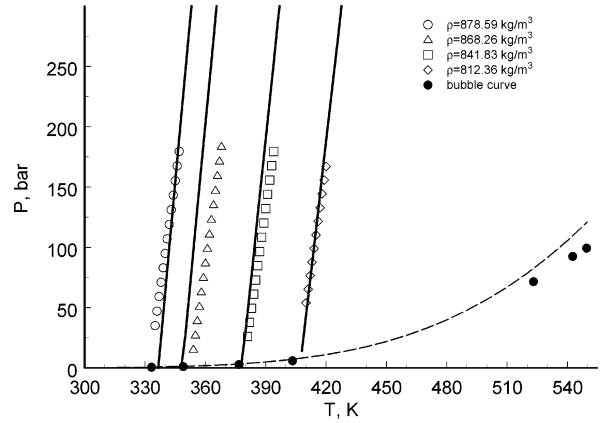

Figure 9. One-phase $P-T$ isochores[44] (empty symbols) and bubble curve saturated pressure data[46] (filled symbols) for water + methanol mixture with predictions of the HRX-SAFT model (curves).

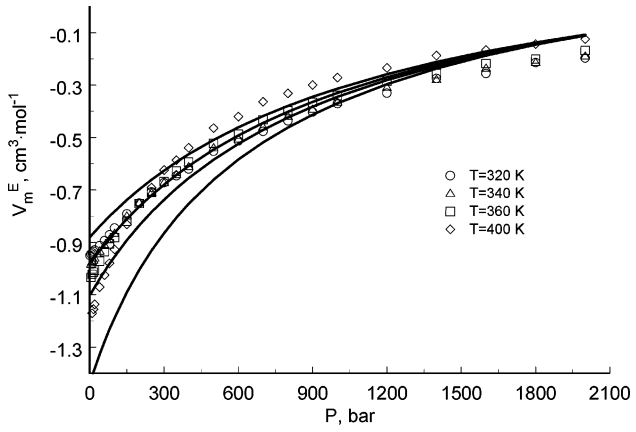

Figure 10. Molar volume V_m as a function of pressure for water + methanol mixture at $x = 0.4993$ mol % of methanol and different temperatures. The curves correspond to the HRX-SAFT model, and the symbols indicate the experimental data obtained by Osada et al.[61]

atures, the critical locus of the liquid−liquid equilibrium in this mixture starts from the critical point of pure water and tends to higher pressures as the temperature decreases. In general, the crossover behavior in higher types of mixtures is more complicated than for the Type I mixtures considered above,[48,49] and we will not consider it here. In this work, we will just show that the HRX-SAFT model is capable of giving an accurate and

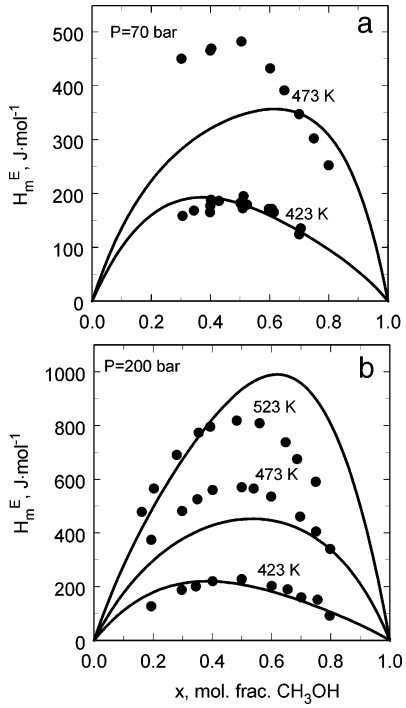

Figure 11. Excess molar enthalpy H_m^E as a function of composition for water + methanol mixture at $P = 70$ bar (a) and 200 bar (b) and different temperatures. The curves correspond to the HRX-SAFT model, and the symbols indicate the data of Wormald et al.[62]

thermodynamically self-consistent representation of the excess properties for this type of mixture. The predictions of the HRX-SAFT model for the excess molar volumes are compared with experimental data at 300 and 400 °C and pressures to 1000 bar obtained by Blencoe and co-workers[50,51] in Figures 12 and 13. As one can see, at all pressures higher than 150 bar excellent agreement between calculated values experimental data is observed. Only at pressures $P = 149.4$, 99.4, and 74.7 bar some systematic deviations, comparable with experimental errors, are observed. However, we need to note that even at these pressures the HRX-SAFT EOS gives very good representation of the molar volumes in this mixture. In Figure 14 we show comparisons for the molar volume, V_m, at 673 K and pressures from 50 to 1000 bar. For all points shown in Figure 14, the difference between experimental and calculated values of molar volume

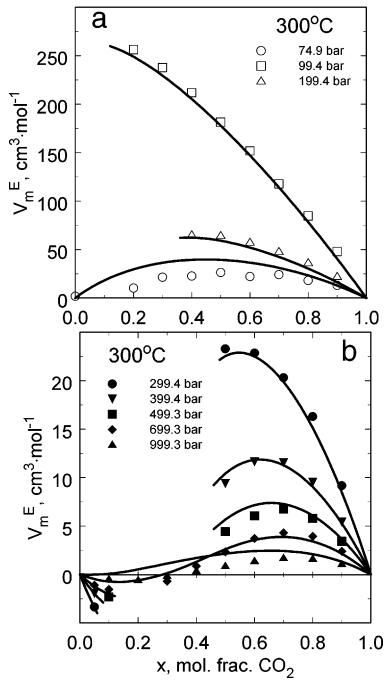

Figure 12. Excess molar volumes V_m^E as a function of pressure for the carbon dioxide + water mixture at 300 °C. The curves correspond to the HRX-SAFT model, and the symbols indicate the experimental data.[51]

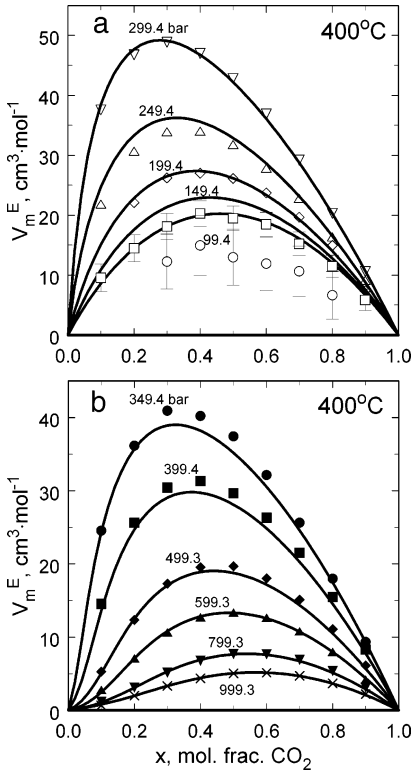

Figure 13. Excess molar volumes V_m^E as a function of pressure for the carbon dioxide + water mixture at 400 °C. The curves correspond to the HRX-SAFT model, and the symbols indicate the experimental data.[50]

does not exceed 2−3%, or $\delta V_m \cong 10-20$ cm^3 × mol^{-1} at $P =$ 50−150 bar, that approximately correspond to the values the excess molar volumes V_m^E at this pressures. Therefore, the results presented in Figures 12 and 13 at these pressures are reasonably good. A comparison of the HRX-SAFT predictions with experimental values of the excess molar enthalpy of

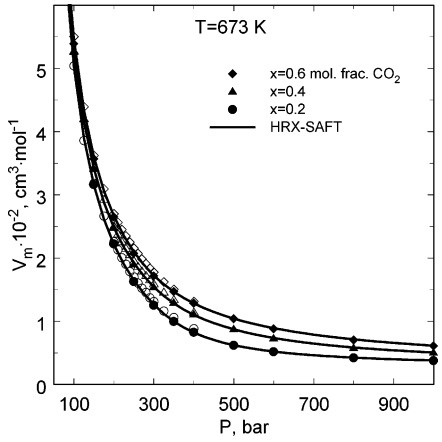

Figure 14. Molar volume V_m as a function of pressure for the carbon dioxide + water mixture at 673 K and different compositions. The curves correspond to the HRX-SAFT model, and the symbols indicate the experimental data obtained by Seitz et al.[50] (empty) and by Abdulagatov et at.[63] (filled).

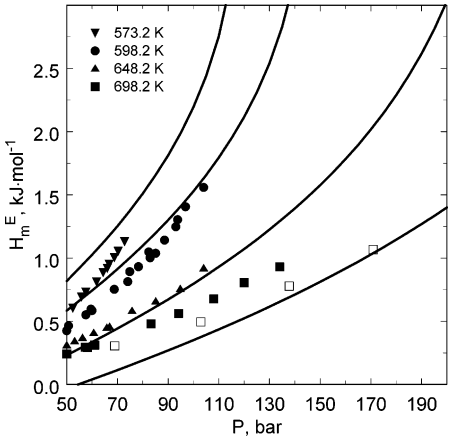

Figure 15. Excess molar enthalpy H_m^E as a function of pressure for the equimolar carbon dioxide + water mixture at different temperatures. The curves correspond to the HRX-SAFT model, and the symbols indicate the original data of Wormald et al.[52] (filled) and the values calculated by Wormald et al.[52] from the measurements of Wilson and Brady[64] (empty).

equimolar $CO_2 + H_2O$ mixture obtained by Wormald et al.[52] is shown in Figure 15. Generally good agreement between experimental data and calculated values of the excess molar enthalpy is observed.

4. Conclusion

In this work, by incorporating classical composition dependent mixing rules into the crossover HR-SAFT EOS for pure fluids developed earlier,[22] we developed a HRX-SAFT EOS for mixtures of associating fluids. We show that the HRX-SAFT EOS not only reproduces better the VLE properties of binary mixtures in the critical region than a classical HR-SAFT EOS but also yields a very good description of the excess properties as well.

Acknowledgment

The research in the Colorado School of Mines was supported by the U.S. Department of Energy, Office of Basic Energy Sciences, under Grant DE-FG03-95ER14568. The research in the University of Wyoming was supported by the University of Wyoming's Enhanced Oil Recovery Institute.

Appendix

The third-order derivatives of the fractions of nonbonded associating molecules:

$$[\mathbf{\Lambda}_{pq}]\left(\frac{\partial^3}{\partial\xi\,\partial\omega\,\partial\theta}[X_i^j]\right) = [\mathbf{\Psi}_p^{\xi\omega\theta}]$$

1. With respect to density: $\partial^3 X_i^j/\partial\rho^3$:

$$\mathbf{\Psi}_p^{\rho\rho\rho} = \frac{3}{\rho}\frac{\partial^2 X_i^j}{\partial\rho^2} - \frac{6}{\rho^3}X_i^j(1-X_i^j) + \frac{6}{X_i^j}\left(\frac{\partial X_i^j}{\partial\rho}\frac{\partial^2 X_i^j}{\partial\rho^2} - \frac{1}{X_i^j}\left(\frac{\partial X_i^j}{\partial\rho}\right)^3\right) - \frac{6}{\rho}\frac{\partial X_i^j}{\partial\rho}\left(\frac{1}{\rho} + \frac{1}{X_i^j}\frac{\partial X_i^j}{\partial\rho}\right) - \rho(X_i^j)^2\sum_{k=1}^{n} x_k \sum_{l=1,l\neq j}^{s} S_k^l\left(X_k^l\frac{\partial^3\Delta_{ki}^{lj}}{\partial\rho^3} + 3\frac{\partial^2\Delta_{ki}^{lj}}{\partial\rho^2}\frac{\partial X_k^l}{\partial\rho} + 3\frac{\partial\Delta_{ki}^{lj}}{\partial\rho}\frac{\partial^2 X_k^l}{\partial\rho^2}\right)$$

2. With respect to density and temperature: $\partial^3 X_i^j/\partial\rho\partial T^2$:

$$\mathbf{\Psi}_p^{\rho TT} = \frac{1}{\rho}\frac{\partial^2 X_i^j}{\partial T^2} - \frac{2}{\rho X_i^j}\left(\frac{\partial X_i^j}{\partial T}\right)^2 + \frac{2}{X_i^j}\left(\frac{\partial X_i^j}{\partial\rho}\frac{\partial^2 X_i^j}{\partial T^2} - \frac{3}{X_i^j}\frac{\partial X_i^j}{\partial\rho}\left(\frac{\partial X_i^j}{\partial T}\right)^2 + 2\frac{\partial X_i^j}{\partial T}\frac{\partial^2 X_i^j}{\partial\rho\partial T}\right) - \rho(X_i^j)^2\sum_{k=1}^{n} x_k \sum_{l=1,l\neq j}^{s} S_k^l\left(X_k^l\frac{\partial^3\Delta_{ki}^{lj}}{\partial\rho\partial T^2} + 2\frac{\partial^2\Delta_{ki}^{lj}}{\partial\rho\partial T}\frac{\partial X_k^l}{\partial T} + 2\frac{\partial\Delta_{ki}^{lj}}{\partial T}\frac{\partial^2 X_k^l}{\partial\rho\partial T} + \frac{\partial X_k^l}{\partial\rho}\frac{\partial^2\Delta_{ki}^{lj}}{\partial T^2} + \frac{\partial\Delta_{ki}^{lj}}{\partial\rho}\frac{\partial^2 X_k^l}{\partial T^2}\right)$$

Literature Cited

(1) Jackson, G.; Chapman, W. G.; Gubbins, K. E. *Mol. Phys.* **1988**, *65*, 1−31.

(2) Chapman, W. G.; Gubbins, K. E.; Jackson, G.; Radosz, M. *Fluid Phase Equilib.* **1989**, *52*, 31−38.

(3) Chapman, W. G.; Gubbins, K. E.; Jackson, G.; Radosz, M. *Ind. Eng. Chem. Res.* **1990**, *29*, 1709−1721.

(4) Huang, S. H.; Radosz, M. *Ind. Eng. Chem. Res.* **1990**, *29*, 2284−2294.

(5) Huang, S. H.; Radosz, M. *Fluid Phase Equilib.* **1991**, *70*, 33−54.

(6) Huang, S. H.; Radosz, M. *Ind. Eng. Chem. Res.* **1991**, *30*, 1994−2005.

(7) Fu, Y.-H.; Sandler, S. I. *Ind. Eng. Chem. Res.* **1995**, *34*, 1897−1996.

(8) Kraska, T.; Gubbins, K. E. *Ind. Eng. Chem. Res.* **1996**, *35*, 4727−4737.

(9) Wertheim, M. S. *J. Stat. Phys.* **1984**, *35*, 19−34.

(10) Wertheim, M. S. *J. Stat. Phys.* **1984**, *35*, 35−47.

(11) Wertheim, M. S. *J. Stat. Phys.* **1986**, *42*, 459−476.

(12) Wertheim, M. S. *J. Stat. Phys.* **1986**, *42*, 477−492.

(13) Paricaud, P.; Galindo, A.; Jackson, G. *Fluid Phase Equilib.* **2002**, *194−197*, 87−96.

(14) Muller, E. A.; Gubbins, K. E. *Ind. Eng. Chem. Res.* **2001**, *40*, 2193−2211.

(15) Anisimov, M. A.; Kiselev, S. B.; Sengers, J. V.; Tang, S. *Physica A* **1992**, *188*, 487−525.

(16) Kiselev, S. B. *Fluid Phase Equilib.* **1998**, *147*, 7−23.

(17) Kudelkova, L.; Lovland, J.; Vonka, P. *Fluid Phase Equilib.* **2002**, *218*, 103−112.

(18) Kiselev, S. B.; Friend, D. G. *Fluid Phase Equilib.* **1999**, *162*, 51−82.

(19) Kiselev, S. B.; Ely, J. F. *J. Chem. Phys.* **2003**, *119*, 8645−62.

(20) Kiselev, S. B.; Ely, J. F. *Fluid Phase Equilib.* **2004**, *222/223*, 149−159.

(21) Kiselev, S. B.; Ely, J. F. *Ind. Eng. Chem. Res.* **1999**, *38*, 4993−5004.

(22) Kiselev, S. B.; Ely, J. F.; Adidharma, H.; Radosz, M. *Fluid. Phase. Equilib.* **2001**, *183−184*, 53−64.

(23) Hu, Z.-Q.; Yang, J.-C.; Li, Y.-G. *Fluid Phase Equilib.* **2003**, *205*, 1−15.

(24) Hu, Z.-Q.; Yang, J.-C.; Li, Y.-G. *Fluid Phase Equilib.* **2003**, *205*, 25−36.

(25) McCabe, C.; Kiselev, S. B. *Fluid Phase Equilib.* **2004**, *219*, 3.

(26) McCabe, C.; Kiselev, S. B. *Ind. Eng. Chem. Res.* **2004**, *43*, 2839.

(27) Sun, L.; Kiselev, S. B.; Ely, J. F. *Fluid Phase Equilib.* **2005**, *233*, 270−285.

(28) Mansoori, G. A.; Carnahan, N. F.; Starling, K. E.; Leland, T. W. *J. Chem. Phys.* **1971**, *54*, 1523.

(29) Chen, S. S.; Kreglewski, A. *Ber. Bunsen-Ges. Phys. Chem.* **1977**, *81*, 1048−1051.

(30) Tan, S. P.; Adidharma, H.; Radosz, M. *Ind. Eng. Chem. Res.* **2004**, *43*, 203−208.

(31) Kiselev, S. B.; Ely, J. F.; Abdulagatov, I. M.; Magee, J. W. *Int. J. Thermophys.* **2000**, *6*, 1373−1405.

(32) Anisimov, M. A.; Kiselev, S. B. In *Soviet Technology Reviews, Section B, Thermal Physics, Part 2*; Scheindlin, A. E., Fortov, V. E., Eds.; Harwood Academic: New York, 1992; Vol. 3.

(33) Sengers, J. V.; Levelt Sengers, J. M. H. *Annu. Rev. Phys. Chem.* **1986**, *37*, 189−222.

(34) Kiselev, S. B.; Ely, J. F. *Fluid Phase Equilib.* **2000**, *174*, 93−119.

(35) Fisher, M. *Phys. Rev.* **1968**, *176*, 257−271.

(36) Griffiths, R. B.; Wheeler, J. C. *Phys. Rev. A* **1970**, *2*, 1047−1064.

(37) Saam, W. F. *Phys. Rev. A* **1970**, *2*, 1461−1466.

(38) Sun, L.; Zhao, H.; Kiselev, S. B.; McCabe, C. *J. Phys. Chem. B* **2005**, *109*, 9047−9058.

(39) Button, J. K.; Gubbins, K. E. *Fluid Phase Equilib.* **1999**, *158−160*, 175−181.

(40) *Release of the IAPWS Formulation 1995 for the Thermodynamic Properties of Ordinary Water Substance for General and Scientific Use*: Frederica, Denmark, 1996.

(41) Leu, A.-D.; Chung, S. Y.-K.; Robinson, D. B. *J. Chem. Thermodyn.* **1991**, *23*, 979−985.

(42) Kiselev, S. B.; Belyakov, M. Y.; Rainwater, J. C. *Fluid Phase Equilib.* **1998**, *150*, 439−449.

(43) Shahverdiev, A. N.; Safarov, J. T. *Phys. Chem. Chem. Phys.* **2002**, *4*, 979−986.

(44) Aliev, M. M.; Magee, J. W.; Abdulagatov, I. M. *Int. J. Thermophys.* **2003**, *24*, 1551−79.

(45) Bazaev, A. R.; Abdulagatov, I. M.; Magee, J. W.; Bazaev, E. A. *Int. J. Thermophys.* (manuscript in preparation).

(46) Bazaev, A. R.; Abdulagatov, I. M.; Magee, J. W.; Bazaev, E. A.; Ramazanova, A. E.; Abdurashidova, A. A. *Int. J. Thermophys.* **2004**, *25*, 805-.

(47) Van Konynenberg, P. H.; Scott, R. L. *Philos. Trans. R. Soc. London* **1980**, *298*, 495.

(48) Anisimov, M. A.; Gorodetskii, E. E.; Kulikov, V. D.; Povodyrev, A. A.; Sengers, J. V. *Physica A* **1995**, *220*.

(49) Rainwater, J. C. *Int. J. Thermophys.* **2000**, *21*, 719−737.

(50) Seitz, J. C.; Blencoe, G. *Geochim. Cosmochim. Acta* **1999**, *63*, 1559−69.

(51) Singh, J.; Blencoe, G.; Anovitz, M. In *Steam, Water, and Hydrothermal Systems*, Proceedings of the 13th International Conference on the Properties of Water and Steam; Tremaine, P. R., Irish, D. E., Balakrishnan, P. V., Eds.; NRC Research Press: Toronto, Canada, 2000.

(52) Wormald, C. J.; Lancaster, N. M.; Sellars, A. J. *J. Chem. Thermodyn.* **1986**, *18*, 135−147.

(53) Duschek, W.; Kleinrahm, R.; Wagner, W. *J. Chem. Thermodyn.* **1990**, *22*, 827−841.

(54) Gilgen, R.; Kleinrahm, R.; Wagner, W. *J. Chem. Thermodyn.* **1992**, *24*, 1243−1250.

(55) Rivkin, S. L.; Akhundov, T. S. *Teploenergetika (Russian)* **1962**, *9*, 57.

(56) Rivkin, S. L.; Akhundov, T. S. *Teploenergetika (Russian)* **1963**, *10*, 66.

(57) Rivkin, S. L.; Troyanovskaya, G. V. *Teploenergetika (Russian)* **1964**, *11*, 72.

(58) Rivkin, S. L.; Akhundov, T. S.; Kremenevskaya, E. A.; Asadullaeva, N. N. *Teploenergetika (Russian)* **1966**, *13*, 59.

(59) Vargaftik, N. B.; Filippov, L. P.; Tarzimanov, A. A.; Totskii, E. E. *Handbook of Thermal Conductivity of Liquids and Gases*; CRC Press: Boca Raton, FL, 1994.

(60) Brunner, E.; Hultenschmidt, W.; Schlichtharle, G. *J. Chem. Thermodyn.* **197**, *19*, 273−291.

(61) Osada, O.; Sato, M.; Uematsu, M. *J. Chem. Thermodyn.* **1999**, *31*, 451−463.

(62) Wormald, C. J.; Badock, L.; Lloyd, M. J. *J. Chem. Thermodyn.* **1996**, *28*, 603−613.

(63) Abdulagatov, I. M.; Bazaev, A. R.; Ramazanova, A. E.; Gasanov, R. K. In *Physical Chemistry of Aqueous System*: *Meeting the Needs of Industry*, Proceedings of the 12th International Conference on the Properties of Water and Steam; White, H. J., Sengers, J. V., Neumann, D. B., Bellows, J. C., Eds.; NRC Research Press: Toronto, Canada, 1995.

(64) Wilson, G. M.; Brady, C. J. Gas Processors Association Research Report 73. Tulsa, OK, 1983.

Received for review October 31, 2005
Accepted March 21, 2006

IE0512082